
Pleating and irreversible deformation of a flat, stretched, sheet at non-zero temperatures

Saswati Ganguly^{*a}, Debankur Das^b, Jürgen Horbach^a, Peter Sollich^c, Smarajit Karmakar^b and Surajit Sengupta^b

We study the emergence of pleats in a stretched two-dimensional sheet composed of connected vertices arranged as a regular triangular lattice. We consider only “flat-foldable” pleats i.e. those with all displacements restricted to the two-dimensional plane. Pleats occur here as a result of an equilibrium first order transition from the homogeneous sheet to a heterogeneous phase where stress is localised within pleats and eliminated elsewhere. To facilitate pleating, we introduce an external field which couples to local *non-affine* displacements i.e. those displacements of neighbouring vertices which cannot be represented as a local affine strain. We obtain both zero and finite temperature phase diagrams in the strain-field plane. We show that in the thermodynamic limit the un-pleated state is always metastable at vanishing field for infinitesimal strain. Plastic deformation of an un-pleated sheet is akin to decay of a metastable phase via a dynamical transition. Our predictions regarding equilibrium and dynamics of the pleating transition, local stress distributions and thermal effects associated with pleats may be verified experimentally.

1 Introduction

There has recently been a lot of interest in structures which may be constructed by pleating or folding (origami)¹ or cutting and subsequent joining (kirigami)^{2,3} of two-dimensional sheets. Such studies are useful both as a response to the technological need for fabricating complex shapes from simple components as well as to understand naturally occurring folded designs in the living world^{1,4-9,16,17}. A special class among these shapes consists of the so-called “flat foldable” configurations which can be unfolded from a two-dimensional to a three-dimensional shape by changing a single parameter^{10,11}. Such flat foldable origami can be constructed as a series of complex hierarchical patterns involving intersecting pleats - so called Miura Ori tessellations^{1,10}. Most of our theoretical understanding of these structures comes from analyses based on the elasticity of thin plates and sheets⁵⁻⁸. Normally, a *finite*-sized flat sheet of elastic material pleats in response to the constraint arising from the requirement that it sticks as close as possible to a substrate which has a curvature^{5-8,10}. A constrained elastic energy minimisation then yields most of the pleated or wrinkled structures seen in experiments⁸.

These studies are *athermal* i.e. thermal fluctuations and entropic contributions arising from them are neglected. Such an approximation is indeed valid for the relatively large, stiff, sheets used in the corresponding experiments⁸. However, we may easily envisage situations where pleated, crumpled

or wrinkled states are produced by self-organizing polymeric membranes¹². In the case of origami structures produced from sheets at small length scales made out of soft materials in the presence of strong Brownian motion¹³ arising from a solvent medium, thermal fluctuations need to be accounted for.

In this paper, we take this complementary viewpoint, regarding the pleating process as a finite temperature phase transition associated with a spontaneous breaking of translational invariance. This phase transition occurs under the influence of a field h_X which can either promote or suppress pleating of a sheet, depending on the sign of h_X . Thus we treat the sheet as a bulk two-dimensional (2d) thermodynamic system.

In a recent paper¹⁴ some of us showed that flat-foldable patterns are obtained as distinct minima of a statistical mechanical free energy in an unstrained sheet. In this paper, we extend this earlier study and investigate the pleating transition as the sheet is subjected to an area preserving uniaxial tensile strain along one of its two dimensions. Our emphasis, in this work, is on the mechanical behaviour and plastic deformation of the pleated state. Many properties of pleats vary smoothly in the limit $h_X \rightarrow 0$ allowing us to make predictions for this experimentally accessible limit.

We represent a 2d sheet by a network of vertices connected by bonds. Such a sheet can produce flat pleats if the potential energy depends on the length of the bonds alone and bond bending costs no energy¹⁵ - a so-called “phantom” network^{18,19}. This process is illustrated in Fig.1 where we have shown the formation of pleats. In the final configuration no bond is stretched and therefore there is no extensive elastic energy cost for pleating in the thermodynamic limit. Figure. 1 also shows how pleating in more than one direction can be combined to construct complex patterns. The pleated regions

^a Institut für Theoretische Physik II: Weiche Materie, Heinrich Heine-Universität Düsseldorf, Universitätsstraße 1, 40225 Düsseldorf, Germany.

^b TIFR Centre for Interdisciplinary Sciences, 36/P Gopanapally, Hyderabad 500107, India.

^c King's College London, Department of Mathematics, Strand, London WC2R 2LS, UK.

have large values of the parameter χ , a local quantity to be defined later, whose spatial average is thermodynamically conjugate to h_X .

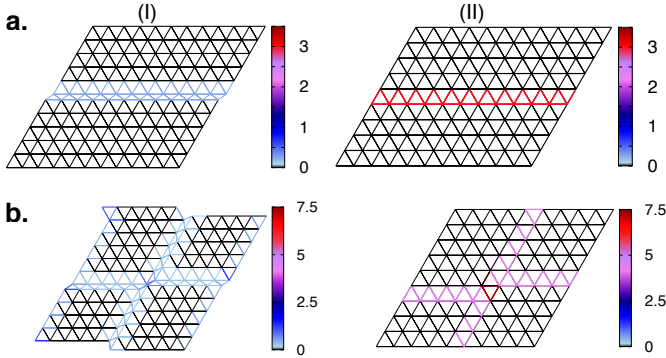


Fig. 1 Intermediate (I) and final (II) stages of system spanning pleats produced by displacing vertices in 2d of a regular triangular network of bonds (lines). To reduce boundary effects, we use a periodically repeated *rhombus* as the initial shape of the network in this calculation. In the final structure, each pleat consists of a pair of overlapped vertex rows. Both a single horizontal pleat, **a**, and a double pleat, **b**, are shown. The bonds are coloured according to the local χ or non-affinity (see text).

It is straightforward to imagine the pleated patterns as shown in Fig. 1 and those constructed by combining these to be flat folded, 2d, versions of Miura Ori origami which have been extensively studied^{10,11}.

Our main results are as follows. We show that the phase transition observed previously¹⁴ persists for non-zero uniaxial strain. Indeed, we find that in the thermodynamic limit the un-pleated sheet under *infinitesimal* strain is metastable with respect to the spontaneous formation of pleats for $h_X \rightarrow 0$. In a finite system, under the same conditions, the un-pleated state is stable upto a non-zero value of strain. As in the zero strain version¹⁴, the pleated and the un-pleated states exist across a well-defined interface produced by differing values of the local stress. The barrier between the coexisting states is large and the un-pleated sheet can exist as a long-lived metastable state well within the region of the equilibrium phase diagram where the pleated phase is stable. Plastic deformation of the sheet during stretching can be viewed as the decay of this metastable state. We also study the local structure of a pleat and metastability of the pleated phase in the $h_X \rightarrow 0$ limit. We use a variety of computer simulation techniques such as Monte Carlo²⁰ and molecular dynamics (MD)^{21,22} as well as sequential umbrella sampling²³ to arrive at these results.

The rest of the paper is organised as follows. In the next section (Section 2) we introduce our model for the two-

dimensional sheet and define χ and h_X . This is followed by the computation of the zero-temperature phase diagram and discussion of the thermodynamic limit. In Section 3 we discuss the equilibrium pleating transition at non-zero temperatures for a finite sized sheet using sequential umbrella sampling Monte Carlo (SUS-MC)²³ simulations. We also study in detail the local structure of the pleat. Next, in Section 4 we discuss dynamics of pleating and plastic deformation of the sheet and aspects of metastability. Finally we conclude the paper in Section 5 mentioning some possible experimental consequences of our work and future directions of research.

2 Sheet, pleats and energy minimization

2.1 The model 2d sheet and non-affine displacements

In order to represent a 2d sheet, we choose a reference lattice structure $\{\mathbf{R}_i\}_{i=1,\dots,N}$ corresponding to an ideal triangular lattice. The (point) vertices of this lattice are then connected by harmonic bonds¹⁵. In an earlier paper¹⁴ we have shown that self-avoidance of vertices modelled by attaching repulsive particles do not change conclusions qualitatively. We therefore consider the following harmonic network model:

$$\mathcal{H}_0 = \sum_{i=1}^N \frac{\mathbf{p}_i^2}{2m} + \frac{K}{2} \sum_{i=1}^N \sum_{j \in \Omega_i, i < j} (|\mathbf{r}_j - \mathbf{r}_i| - |\mathbf{R}_j - \mathbf{R}_i|)^2$$

where \mathbf{p}_i is the momentum, m the mass, \mathbf{r}_i the instantaneous position, and \mathbf{R}_i the reference position of vertex i . The length and energy scales are set by the lattice parameter l and Kl^2 respectively. The time scale is set by $\sqrt{m/K}$. In our calculations, we set $l = 1$, $m = 1$, $K = 1$. The dimensionless inverse temperature $\beta = Kl^2/k_B T$, with k_B the Boltzmann constant.

The formation of pleats requires *non-affine* displacements, namely those displacements of particles which cannot be represented as an affine transformation of the reference configuration. The statistics of such displacements have been studied extensively in crystals^{24,25} and glasses²⁶. We begin this section by giving below a brief description of non-affineness relevant to our present work.

The local non affine parameter $\chi(\mathbf{R}_i)$ is defined as the least squares error encountered on trying to fit a “best fit” local affine deformation D_i to the set of *relative* vertex displacements within a coarse graining volume Ω_i around vertex i ²⁴. Related to this local non-affine parameter, we can define the global non-affine parameter $X = N^{-1} \sum_i \chi(\mathbf{R}_i)$ where N is the number of vertices used to represent the sheet. In Ref.²⁵ we have shown that this quantity behaves as a standard thermodynamic variable permitting a conjugate field h_X which may enter the microscopic Hamiltonian as

$$\mathcal{H} = \mathcal{H}_0 - N h_X X, \quad (1)$$

We use the full Hamiltonian \mathcal{H} in Eq.(1) to model the 2d sheet and obtain the results which follow. The non-affine field h_X and the conjugate density X have an intriguing correspondence with stress and strain. This has been shown²⁴ to result from projecting all possible relative vertex displacements within Ω into mutually orthogonal *affine* and non-affine components.

The affine part of the displacements give rise to the three independent components of the symmetric strain tensor $\varepsilon_{\mu\nu}$ and their conjugate stresses $\sigma_{\mu\nu}$ with $\mu, \nu = 1, 2$ being the dimensional indices. We also use the notation $1 \equiv x$ and $2 \equiv y$. Unless otherwise mentioned, we are mostly concerned with the uniaxial strain $\varepsilon_d = \varepsilon_{11} - \varepsilon_{22}$ and conjugate stress $\sigma_d = \sigma_{11} - \sigma_{22}$ which represents a stretching in the x direction with a corresponding contraction in the y direction preserving the area to linear order. The non-affine part, X , of the displacements, on the other hand, couples to h_X .

This projection procedure is an intrinsic part of our definition of χ . An important consequence is the fact that, to linear order, fields conjugate to the non-affine component of the displacements do not affect the affine subspace, and vice versa²⁴. In other words, small h_X do not produce stresses or change elastic constants. Similarly small stresses do not generate non-affine displacements. Lastly, note that χ (and therefore X) depends only on relative displacements and making Eq.(1) *translationally invariant*. Spatial heterogeneity can therefore arise only if translational symmetry is *spontaneously* broken due to a thermodynamic phase transition as we shall see in Section 3.

2.2 The zero-temperature phase diagram

Before we describe finite temperature phase transformations in the next section, we use the Hamiltonian 1 to study the relative stability of pleated states at $T = 0$. In this limit, simple expressions for the energy of the pleated configuration can be derived as a function of ε_d , and h_X .

The un-pleated lattice, taken as reference, has the shape of a periodically repeated rhombus of sides L_y and L_x taking x as the horizontal direction and y along a line making an angle of 60° with x , commensurate with a triangular lattice. We found this coordinate system to be most suited for the calculations reported in this section because pleats along all three symmetry axes of the triangular lattice are treated equivalently. In later sections for the simulation results we have chosen the usual commensurate rectangular box and Cartesian coordinates.

To produce pleats (see Fig. 1) we displace a full row of vertices towards an adjacent parallel row, continuing the displacement till exactly two rows overlap. In this state, no bond is stretched and any elastic component of the energy of the sheet is non-extensive and therefore negligible. Considering, for the moment only parallel horizontal pleats, in a finite sheet, this

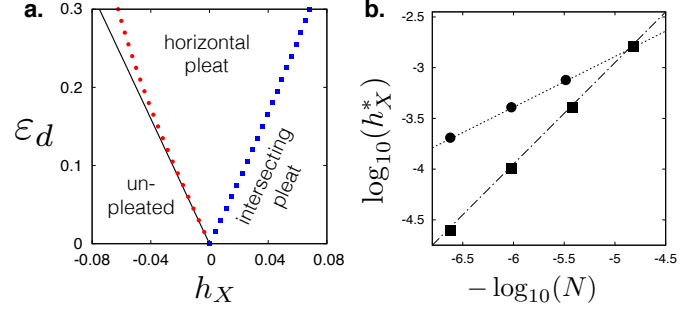


Fig. 2 a. The $T = 0$ phase diagram in the $\varepsilon_d - h_X$ obtained by numerically minimising the total energy for a 2d flat sheet modelled as network with 2048×2048 vertices. We consider the un-pleated sheet as well as sheets with a single horizontal pleat and two intersecting pleats (see Fig. 1). The red and blue symbols mark the respective phase boundaries while the black straight line is a result from analytic calculations. **b.** Plot of the h_X^* vs N in logarithmic scale where h_X^* is the value of the field at the transition point between an un-pleated sheet and one with a single pleat at $\varepsilon_d = 0$. Note that as $N \rightarrow \infty$, $h_X^* \rightarrow 0$; the two curves representing two different protocols for taking the thermodynamic limit. If L_x is kept constant then $h_X^* \sim 1/N$ (■), whereas if L_x and L_y are scaled proportionately, $h_X^* \sim 1/\sqrt{N}$ (●), as expected.

operation reduces the length in the y direction by the combined width of the pleats. To compare equal areas, we need to scale the lattice in the y direction to preserve L_y . This operation produces an internal strain $\varepsilon_{22}^{\text{int}} \equiv \varepsilon^{\text{int}} = 2n_p/(1 - 2n_p)$, where n_p is the number of pleats per unit length in the y direction. Usually, $n_p \ll 1$ and so $\varepsilon^{\text{int}} \approx 2n_p$. The pleated region also produces local non-affinity χ_p which is same for all vertices taking part in the pleat. Therefore, the globally averaged non-affine parameter $X = 2n_p\chi_p \approx \varepsilon^{\text{int}}\chi_p$. In addition, an external strain ε_d stretches bonds in both the un-pleated and pleated sheets. Collecting together after neglecting higher order terms e.g. $\propto \varepsilon^{\text{int}}\varepsilon_d^2$ etc., we get the energy of the pleated sheet relative to the un-pleated one,

$$\Delta E = \frac{5}{8} (\varepsilon^{\text{int}})^2 - \frac{3}{4} \varepsilon^{\text{int}} \varepsilon_d - h_X \varepsilon^{\text{int}} \chi_p.$$

The numerical coefficients arise from expanding ΔE upto quadratic order in ε^{int} and summing contributions over the nearest neighbour bonds in the triangular lattice.

The linear density of pleats n_p depends on the external strain and can be found by minimising ΔE with respect to ε^{int} which gives,

$$n_p = \frac{2}{5} \left(\frac{3}{4} \varepsilon_d + h_X \chi_p \right),$$

with $n_p \geq 0$ in the pleated phase. For the limiting case $n_p = 0$ we get, for the phase boundary $\Delta E = 0$ the simple expression $h_X = -3\varepsilon_d/4\chi_p$ in the thermodynamic limit.

We have checked some of these results by direct numerical minimisation of the energy for a lattice of 2048×2048 vertices containing either a single horizontal pleat or two intersecting pleats as shown in Fig. 1a and b respectively. The boundary between the un-pleated network and the one containing a single horizontal pleat is compared to the limiting $n_p \rightarrow 0$ phase boundary obtained above.

It is surprising that in the thermodynamic limit, the un-pleated sheet is *metastable* for *all* values of $\varepsilon_d > 0$ for $h_X = 0$! In order to obtain a thermodynamically stable un-pleated sheet, one needs to turn on a negative h_X in order to suppress non-affinity and the resultant pleating. A finite sized sheet, is on the other hand stable for small strains since the phase boundary shifts as a whole to the right as N is decreased. The internal strain $\varepsilon^{\text{int}} \propto n_p \propto 1/L_y$ and therefore the shift of the phase boundaries depend only on L_y . For example, if N is increased keeping the number and length of the pleat constant then the transition points, $h_X^* \sim 1/N$ at $\varepsilon_d = 0$. On the other hand if the area is scaled uniformly, $h_X^* \sim 1/\sqrt{N}$ holds. Our data plotted in Fig. 2b shows that these expectations are validated.

We shall show in the next section that although the un-pleated state is metastable for $\varepsilon_d > 0$ at $h_X = 0$, formation of pleats take a very long time because of large barriers. Similarly, a pleated state, quenched into a region where pleats are not stable takes a long time to decay. Calculations of these barriers are tricky because the most probable path chosen by the system to go from an un-pleated to the pleated structure is *not* through coordinated motion of a complete row of vertices as represented in Fig. 1. Pleats arise from *localised* non-affine deformations as we show below.

3 Results: The equilibrium transition at non-zero temperatures

To study the equilibrium pleating transition as a function of h_X and ε_d at non-zero temperatures, we need efficient computational schemes, which are able to access pleated structures starting from an un-pleated sheet. The reason being that transition probabilities between these two states are vanishingly small due to large barriers. One of the methods which produces satisfactory results in this case is the sequential umbrella sampling Monte Carlo (SUS-MC) technique²³. We use the same SUS-MC technique used earlier to study pleating of the un-stretched sheet¹⁴.

3.1 Sequential umbrella sampling

To implement SUS-MC for our system, we divide the transition coordinate X into small windows and sample configurations generated by Metropolis Monte Carlo^{20,23} in each window successively beginning with $X = 0$, keeping track of how

often the system tries to leave the window via its left or right boundaries in histograms. The probability distribution $P(X)$ can then be computed from these histograms. Further details of this procedure can be obtained from our earlier work¹⁴.

While the SUS-MC technique is quite efficient, the computational effort needed is substantial and grows with N . This restricts the system size that we can study. Fortunately, finite size effects at $T > 0$ follow the same qualitative trend as in the $T = 0$ results discussed in the earlier section 2.2 so conclusions, drawn from studies of small systems can be extrapolated in a straightforward manner. We therefore present results only for $N = 900$ vertices. We use a $\beta = 200$, results at other temperatures are qualitatively similar. The range of $0 < X < 1$ divided into 500 windows gave us sufficient resolution. To obtain sufficiently averaged $P(X)$ values, at least 8×10^7 trial moves were required for *each* window.

We study the sheet in the presence of both h_X and ε_d . Unlike our $T = 0$ calculations where we had a periodically repeated box in the shape of a rhombus, here we have a rectangular box whose dimensions are commensurate with the triangular lattice. The strain is implemented as before by stretching the simulation box along the x -direction and compressing it along the (now vertical) y -direction while conserving area to linear order.

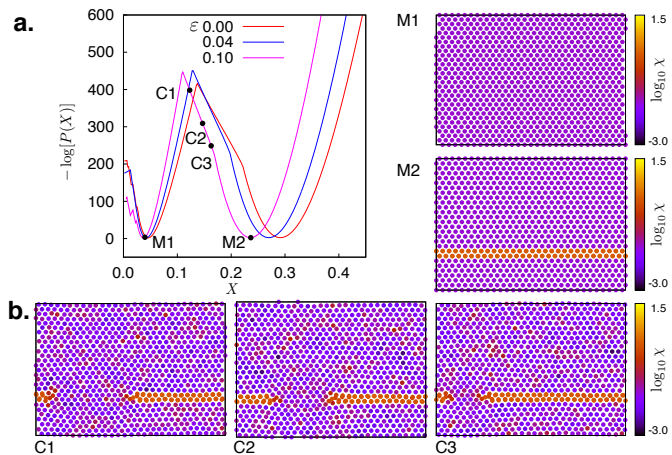


Fig. 3 a. Plot of $-\ln(P(X))$ obtained from sequential umbrella sampling of a 30×30 harmonic lattice for $(\varepsilon_d, h_X) = (0.0, 0.027)$, $(0.04, 0.021)$ and $(0.1, 0.009)$ on the coexistence line. The first minimum M1 corresponds to the perfect lattice while minima M2 corresponds to a configuration with a single horizontal pleat. **b.** Configurations obtained from SUS-MC for $\varepsilon = .10$ at the positions indicated by dots in **a.**

Once $P(X)$ is obtained for any combination of h_X and ε_d value, one can use a histogram reweighting technique²⁸ to determine $P(X)$ at any other h_X . This is particularly useful to obtain the phase boundary in the ε_d - h_X plane.

Fig. 3a, shows $-\ln(P(X))$ for three different h_X and ε_d values close to the phase boundary. While the $\varepsilon_d = 0$ has been studied earlier¹⁴ we include these results here for comparison. Most of the qualitative features are unchanged all along the phase boundary from $\varepsilon_d = 0$ to nonzero values. There are two minima: the ones for small X values (M1) correspond to the un-pleated lattice. Notice that $X \neq 0$ at M1 due to thermal fluctuations. The ensemble average of the un-pleated lattice with harmonic bonds, even under the influence of h_X can be *analytically* obtained²⁴ and offers a stringent test for our calculations. The pleated state has a larger X value (M2) which has contributions from the pleat as well as thermal fluctuations. At higher values of h_X higher order patterns with many pleats are produced. We do not explore these transitions here and concentrate on the transition from the un-pleated sheet to one containing a single horizontal pleat represented by M2.

The usefulness of the SUS-MC method is apparent from Fig. 3 since now we know not only the two co-existing structures but all intermediate ones as well along a transition path quantified by X . This is the optimum (least free energy) path obtained by our Monte Carlo method and shows that the pleat forms by a local transformation which produces a ‘‘lip’’ with two tips which extends all around the periodic boundary and finally annihilates with itself once the pleat percolates through the sheet. This is shown for three configurations at intermediate values of X (C1, C2 and C3) in Fig 3b. At finite external strain the free energy landscape looks qualitatively similar to that for $\varepsilon_d = 0$; in particular, the values of X at which the first two minima occur seem to only weakly depend on ε_d . However, relative to the second minimum the first minimum in $-\ln(P(X))$ moves to higher energies with increasing external strain at fixed h_X . As a consequence, with increasing ε_d one expects a decrease of the coexistence value h_X^* where the phase transition from a homogeneous crystal is expected to happen. The snapshots in Fig. 3b for the case $\varepsilon_d = 0.1$ indicate that the horizontally pleated state grows proportionately (lever rule) as X approaches M2, exactly as expected in a first order transition¹³.

In Fig 4a we show the stress distributions for the three ε_d values chosen earlier and for X corresponding to M1 and M2. The pleated phase always has lower stress. The spatial distribution of stresses for a single configurations corresponding to C1, C2 and C3 as well as for M1 and M2 are shown for $\varepsilon_d = 0.1$ in Fig. 4b. The phases are seen to co-exist across a stress interface which undergoes capillary fluctuations about a mean position. In the M2 phase, the stress becomes heterogeneous and is concentrated mainly in the pleat. Pleats therefore relieve stress from the rest of the sheet concentrating it only within themselves. As the pleat grows the stress interface moves in proportion to the relative amounts of the two phases.

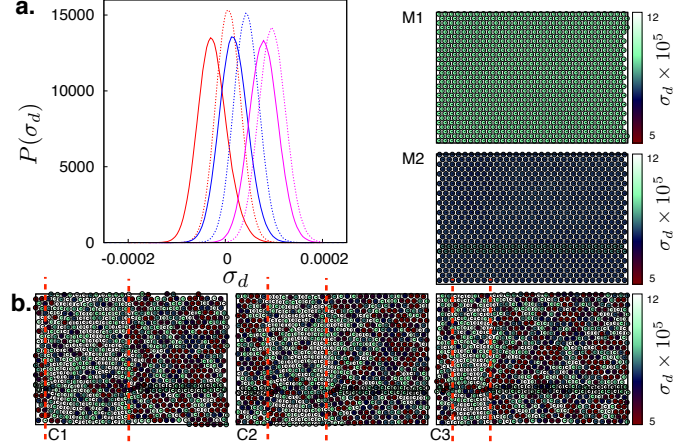


Fig. 4 a. Distribution of local stresses corresponding to the minima M1 (dashed lines) and M2 (solid lines) of the distributions shown in Fig. 3a, the same colour codes are used for the parameter values. **b.** The snapshots correspond to those in Fig. 3 for $\varepsilon = 0.1$, but now the colormap represents the local stresses. Note that these stress maps correspond to a single configuration showing large capillary fluctuations. Red dashed lines mark the average position of the interface.

3.2 Local structure near pleat tips

We now look more closely at the stress distribution near the pleat tips in the C1 and C2 configurations by averaging over many configurations in each of X windows. Since $h_X = 0.009$ is quite small for this state point, the stress distributions should be qualitatively *and quantitatively* accurate even for $h_X = 0$. Our SUS-MC studies therefore allow us to analyse in detail mechanical properties of a pleat in a flat sheet which, as we will see later (Section 4), is nearly impossible to produce using conventional Monte Carlo or molecular dynamics techniques.

We have plotted now all the components of the stress in Fig. 5. The network has also been shown to indicate the position of the pleat. Note that each pleat tip represents a stress dipole with those for the uniaxial stress σ_d being the largest. When the pleat is just about to form, these dipoles are close together forming a quadrupolar pattern. Quadrupolar patterns in the zero stress, two point strain-strain spatial correlation function have been analytically derived earlier²⁴ and this result simply vindicate the fluctuation-response relation¹³. The growth of a pleat is equivalent to a separation of stress dipoles.

To obtain the stress interface quantitatively, we plot σ_d averaged along the y direction as a function of x in Fig 6a for both the C1 and C2 configurations. Note that interfaces have been averaged now over all fluctuations. The width of each interface is about 4 – 5 lattice spacings and remains constant as they move towards each other, again as expected in a first

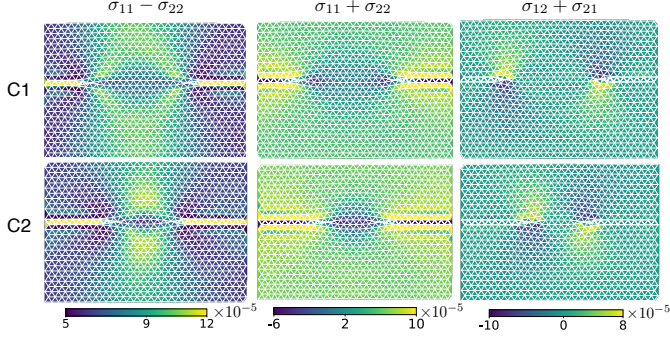


Fig. 5 Local stress maps averaged over 2000 statistically independent well separated configurations for configurations C1 and C2 from Fig. 3. All the three stress components viz. uniaxial $\sigma_d = \sigma_{11} - \sigma_{22}$, pressure $\sigma_{11} + \sigma_{22}$ and shear $\sigma_{12} + \sigma_{21}$ have been plotted.

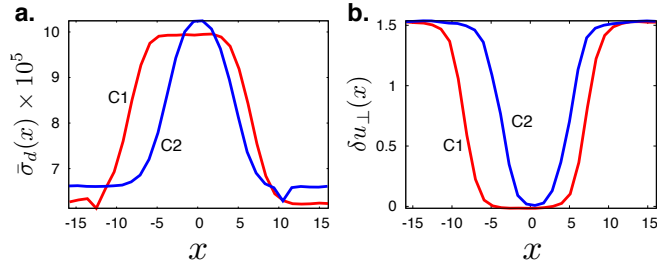


Fig. 6 a. Plot of the uniaxial stress σ_d averaged over 2000 configurations as well as over rows of vertices in the y - direction and plotted along the x direction showing the *mean* stress interface between the un-pleated and the pleated phases. Curves for both the C1 (red line) and C2 (blue line) configurations are shown. **b.** Plot of the relative displacements of vertices perpendicular to the pleat for the C1 and C2 configurations. The colours have the same meaning as in **a.** Note that the stress and the displacement relaxes over the same length scale.

order transition. According to our computations, the interface width does not change along the phase boundary indicating that a critical point is probably absent¹³. In Fig. 6b we have also plotted the relative perpendicular displacement of lattice rows participating in a pleat as a function of x . This quantity rises from zero to the expected value within the pleat. The length scale over which this quantity varies is of the same order as the width of the stress interface.

3.3 The pleating phase diagram

Our results for the equilibrium transition are summarised in the phase diagram Fig 7a where we have shown the equilibrium phase boundaries at non-zero as well as zero temperature

for the same finite system. We have considered only a single horizontal pleat as before. A dynamical transition line, to be discussed later, is also shown. Note that thermal fluctuations *stabilise* the un-pleated phase. Indeed, noting that for $\epsilon_d = 0$ and keeping T and h_X constant, one may write the thermodynamic relation $dU = TdS - h_X dX$ where U is the internal energy and S the entropy of the system. The equality of mixed second derivatives of U then implies a Clausius-Clapyron like relation²⁷,

$$\begin{aligned} \frac{dh_X^*}{dT} &= -\frac{\Delta S}{\Delta X} \\ &= \frac{U_1 - U_2}{T(X_2 - X_1)}, \end{aligned} \quad (2)$$

where U_1 and U_2 refer to the internal energies of the co-existing un-pleated and pleated sheets. The difference in the entropy and the global non-affineness of these co-existing states are represented by ΔS and ΔX respectively. Since $U_1 > U_2$ (see Section 5) and $X_2 > X_1$, the phase boundary should shift to larger values of h_X for the same ϵ_d , as the temperature is increased. This is shown in Fig 7a where we plot, in the same graph a phase boundary obtained at $T = 0$ for a 30×30 network.

4 Results: Metastability, dynamics and deformation

We have mentioned before that high barriers resulting from the formation of highly stressed regions within the sheet where a pleat nucleates (see Fig 3a) prevent the equilibrium transition from occurring in MD simulations within a reasonable time scale.

This is illustrated in Fig. 7b where we have replotted the probability distribution $-\ln P(X)$ from the SUS-MC calculation together with MD simulation²² results for $P(X)$ at $h_X = 0.025$ and $\epsilon = 0.04$. Our MD simulations are performed in the canonical ensemble (constant N , area A and temperature T), using a leapfrog algorithm coupled to a Brown and Clarke thermostat using a time step of 0.002²¹. The MD simulations are started from either an initial un-pleated or pleated state. Within our long simulation time ($\sim 5.0 \times 10^5$ MD steps corresponding to $t = 1000$), there are no fluctuations which connect these states. The free energy barrier separating these states can be seen to be indeed extremely large $\sim 300 - 400k_B T$.

A dynamical transition to a pleated configuration is possible only when h_X becomes sufficiently large so that the lattice is close to being locally unstable and the free energy barrier is substantially reduced. In Fig. 8 a we have plotted h_X against $\langle X \rangle$ obtained from SUS-MC for three different ϵ values. The $\langle X \rangle$ values were obtained by a histogram reweighting method. Together with these results, we have also plotted results from

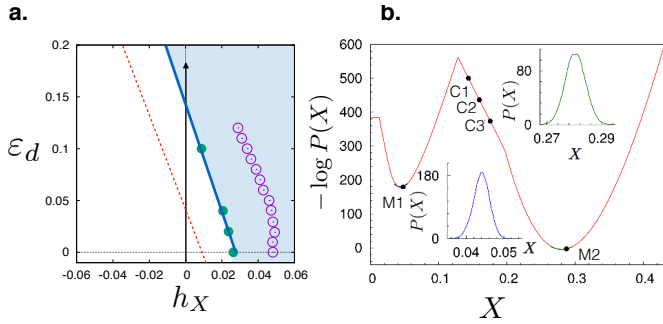


Fig. 7 a. The equilibrium phase diagram for the 30×30 network of vertices. The blue shaded region corresponds to the pleated sheet with one horizontal pleat. The phase boundary between the pleated and un-pleated phases (un-shaded) is shown by the cyan line and symbols. The dynamical transition is shown by purple open circles. Within the region bounded by the phase boundary and the dynamical transition, the un-pleated sheet is in a long-lived metastable state. The $T = 0$ phase boundary (see Section 2) for a finite 900 vertex network is also shown as a red dashed line. **b.** A re-plot of $-\ln(P(X))$ from SUS-MC at $h_X = 0.025$ and $\varepsilon = 0.04$ together with MD results as insets. Inset, plotted in green, shows $P(X)$ obtained from NVT MD simulations for the same parameters with an initial, triangular lattice, configuration $M1$ while the blue line indicates the result when the initial configuration is collected from SUS-MC from the pleated configuration at $M2$. MD simulations sample only a small portion (green and blue patches respectively on the red curve) of the configuration space.

MD simulations of the same network where $\langle X \rangle$ now represents an average over the MD simulation time. The MD and the SUS-MC results both show a jump in $\langle X \rangle$ at the pleating transition. However, the transition in MD occurs at a much larger value of h_X showing that for a large range of h_X , the un-pleated state remains metastable. Our results for the dynamical transitions are also summarised in Fig. 7a as open circles. Within the region in-between the equilibrium and dynamical transition lines the un-pleated state is metastable. The dynamical transition line appears to lie parallel to the equilibrium transition so that there is always a region of metastability (no critical point!) at least within the range of parameter values explored by us.

We plot $\langle X \rangle$ for a number of h_X and ε values in Fig. 8b. This plot shows that the transition shifts to lower values of h_X , following approximately a parabolic shape. At the same time the jump in $\langle X \rangle$ gradually decreases to zero as ε_d is increased. In the equilibrium transition the jump in $\langle X \rangle$ between the un-pleated and pleated states never vanishes and the decrease of $\langle X \rangle$ seen here must be attributed to a purely kinetic effect arising from an arrest of the coarsening process. As the network becomes stiffer with decreasing h_X , growth of $\langle X \rangle$ becomes more and more difficult so that at $h_X = 0$, pleated states

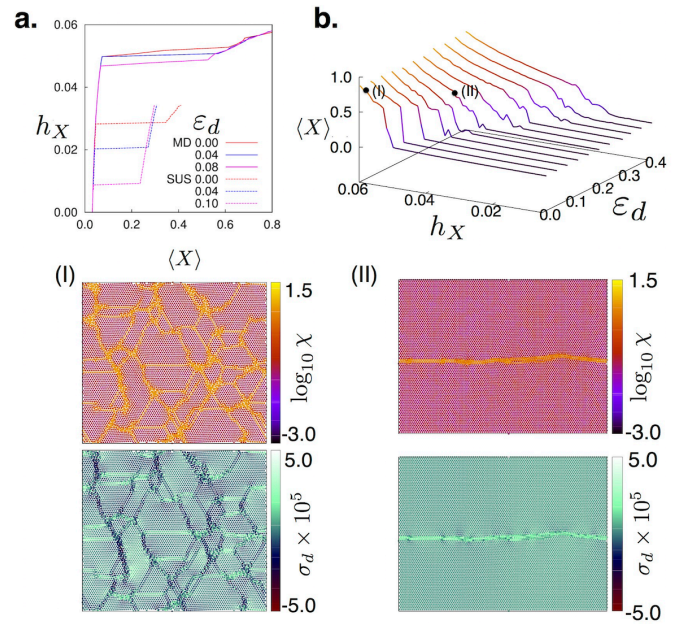


Fig. 8 a. h_X as function of $\langle X \rangle$ corresponding to SUS results for $\varepsilon = 0.0, 0.04$, and 0.10 . These results are compared to the corresponding results from the MD simulations. **b.** Plot of $\langle X \rangle$ from MD simulations as a function of both h_X and strain ε . Note that just before the jump, $\langle X \rangle$ attains a (nearly) constant value. The jump itself decreases with decrease in the value of h_X . (I) and (II) are configurations colored with $\log_{10} \chi$ and $\sigma \times 10^5$ obtained at points indicated by black dots.

do not form and the network remains Hookean for arbitrarily large strains. To understand this, observe the configurations obtained just after the transition plotted in Fig. 8 (I and II) as both local χ and the σ maps for $h_X = 0.06$, $\varepsilon_d = 0.0$ (I) and $h_X = 0.04$, $\varepsilon_d = 0.16$ (II). While, pleated regions of higher local stress similar to the SUS-MC results are seen here, close examination of the configurations suggest that some of the pleated regions are disordered. These structures are arrested since relaxation to the true equilibrium state involving large scale rearrangements take an arbitrary long time.

It is clear from Fig. 8b that the pleated state can be reached either at fixed ε_d by changing h_X or at fixed h_X by increasing ε_d . We show below that the second protocol has many features common to standard yielding transition of solids in the constant strain ensemble²⁹. In Fig. 9a, we plot MD results of the uniaxial stress σ_d on 100×100 lattices for different values of ε_d and h_X . Each of these systems was held at every value of ε_d and h_X for 5.0×10^5 MD steps ($t = 1000$) until there was no perceptible change in the stress values. In this sense, our loading may be considered to be *quasistatic*. For small values of ε_d , the stress is Hookean with a slope given by the elastic constant of the triangular lattice *independent of* h_X ^{24,25}. As the

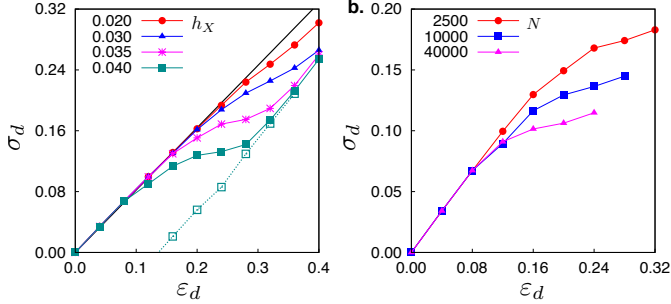


Fig. 9 a. Plots of uniaxial stress σ vs strain from MD simulations of 100×100 lattices at $h_X = .045 - .02$ (filled symbols). The black line shows the Hooke's law behaviour at $h_X = 0.0$. Dotted line with open squares shows value of stress as strain is removed starting from the equilibrated configuration with the highest ϵ . **b.** Plot of σ vs. ϵ for 20×20 , 50×50 , 100×100 , and 200×200 lattices at $h_X = 0.04$. For the smallest lattice sizes, the data was obtained by averaging over many initial conditions. Lines joining data points in all plots above are guides to the eye.

network enters the inhomogeneous phase, the stress deviates from this linear behaviour and pleated states begin to form.

An examination of the configurations suggests that plastic deformation is directly associated with the formation of pleats. When pleat formation is kinetically arrested, at still larger values of ϵ_d the stress again appears to grow linearly with ϵ_d . To show that the pleating transition introduces permanent plastic deformation, we continuously decrease ϵ_d from maximum deformation (Fig. 9a). The strain where σ_d vanishes is non-zero. Irreversible deformation is therefore linked with a breakdown of ergodicity such that the network, once trapped in a pleated state, cannot revert back due to high kinetic barriers.

To show that the dynamical transition is affected by finite system size, we plot in Fig. 9b, σ_d vs. ϵ_d for $h_X = 0.04$ for lattice sizes varying from 50×50 to 200×200 . As system size increases, the transition becomes sharper with value of $\sigma_d(\epsilon_d)$ becoming flatter and more non-linear. However, for larger lattice sizes, the total simulation time $t = 1000$ becomes small compared to the relaxation time of the system and the network gets arrested earlier. Increasing the simulation time algebraically with N does not change these results significantly. Of course, an exponential increase of simulation time with N is beyond the scope of this work.

5 Discussion and conclusions

In this paper we have described in detail pleating and deformation of a two-dimensional sheet under stretching load. We show that the pleating transition is a strongly first order phase transition in the bulk. In order to be able to describe pleating

in this context we needed to define an external field conjugate to a thermodynamic density associated with pleating. The discovery of this variable X viz. the average non-affine parameter is one of the primary contributions of this as well as our earlier¹⁴ work. We show that X also behaves as a reaction coordinate describing the kinetics of pleating starting from local non-affine fluctuations which break centro-symmetry of the lattice^{25,30}.

Recently, some of us have analysed the deformation behaviour of an ideal crystal in 2d in the $h_X - \epsilon$ plane³¹. We conclude that the rigid crystal is always metastable for all $h_X > 0$ and for $h_X < 0$, a first order transition connects the rigid crystal with one which eliminates stress. At coexistence, one observes an interface between the two phases, clearly visible in plots of the stress profile. The interface is created by pairs of dislocations of opposite signs separated by a distance fixed by the lever rule. These observations along with the phase diagram are entirely analogous to what we obtain here. In both cases there is a coexistence between a phase which supports stress and another which eliminates it from the bulk. Also, incipient, non-percolating pleats consisting of two sharp tips connected by a pleated regions, as seen in C1, C2 and C3 configurations (Figs. 3-6) have many similarities with dislocation dipoles. Like the latter, the displacement becomes multi-valued, and therefore non-analytic, within the pleat. These close analogies point to an underlying fundamental link between the two systems. We wish to explore this issue further in the future.

What connection do our results have with actual experiments? First of all, if h_X can be realised experimentally, *all* our results can be verified against actual experimental measurements. A realisation of h_X is actually possible using dynamic, feed-back controlled laser tweezers^{14,25}. However, many of our results are also valid in the limit $h_X \rightarrow 0$. Regardless of how the pleat is obtained, we believe that stress distributions, such as those shown in Fig. 6 should be valid. Finite size effects, again, should be observed similar to that described here. Lastly, if pleating results from a spontaneous self organization as the consequence of a thermodynamic first order transition, then it should be accompanied by thermal effects arising from the release of latent heat²⁷ as we show below.

In Fig.10a, we have plotted the internal energy U averaged over configurations in each window of X for a state on the coexistence line as shown in Fig. 3a. This energy has contributions from both elasticity as well as the part proportional to h_X . This shows that the pleated state has much lower potential energy (about 20%) than the un-pleated sheet for this state at non-zero ϵ_d . There should therefore be a considerable release of energy as the pleat forms.

To see what consequence this may have for the pleating transition in experimental conditions (i.e. for $h_X = 0$), we undertake MD simulations in the canonical ensemble starting

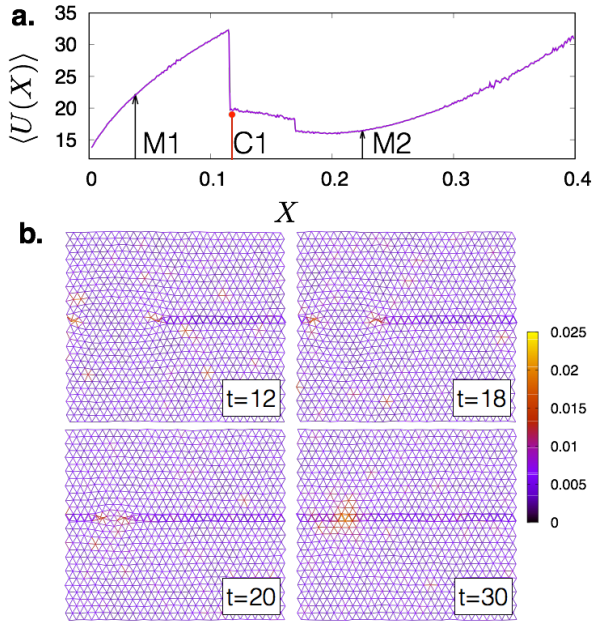


Fig. 10 a. Average internal energy U of configurations at various values of X for $h_X = .009$ and $\epsilon_d = 0.1$. The locations of the M1 and M2 states (black arrows) as well as C1 (red line and dot) are shown. **b.** Snapshots obtained from MD simulations at $h_X = 0$ and $\epsilon_d = 0.1$ starting from the configuration C1 from the SUS-MC calculation (see Fig. 3a) are shown for four different values of time t . The bonds are coloured according to the instantaneous kinetic energy of the vertices. Note the large release of kinetic energy when the pleat completes itself.

from the C1 configuration obtained from our SUS-MC calculation. For these calculations we used the LAMMPS molecular simulation package³². Snapshots from this simulation are presented in Fig. 10b. We observe that the pleat rapidly closes releasing kinetic energy consistent with the expected gain in potential energy as the pleat forms. At least some of this kinetic energy will be converted to heat in a real membrane which will raise its temperature. At large times, of course, these temperature variations disappear. However, for poorly conducting polymeric membranes mentioned in the introduction 1, such heterogeneous temperature variations may be observable near pleats³³. The exact nature of these variations will, of course, depend on the detailed interactions (and consequent thermodynamics) of the system in question and may vary in magnitude as well as sign.

In the future we would like to look at full three-dimensional pleating by including perpendicular vertex displacements as well as the effect of curvature in the presence of h_X and all components of the external strain.

Acknowledgments

Discussions with S. Ghosh and N. Menon are gratefully acknowledged. SS acknowledges support from the FP7-PEOPLE-2013-IRSES grant no: 612707, DIONICOS.

References

- 1 L. Mahadevan and S. Rica, *Science* **307**, 1740 (2005).
- 2 D. M. Sussman, Y. Cho, T. Castle, X. Gong, E. Jung, S. Yang, and R. D. Kamien, *Proc. Natl. Acad. Sci. USA* **112**, 7449 (2015).
- 3 T. Castle, Y. Cho, X. Gong, E. Jung, D. M. Sussman, S. Yang, and R. D. Kamien, *Phys. Rev. Lett.* **113**, 245502 (2014).
- 4 W. T. M. Irvine, V. Vitelli, and P. M. Chaikin, *Nature* **468**, 947 (2010).
- 5 G. M. Grason and B. Davidovitch, *Proc. Natl. Acad. Sci. USA* **110**, 12893 (2013).
- 6 A. Azadi and G. M. Grason, *Phys. Rev. Lett.* **112**, 225502 (2014).
- 7 A. Azadi and G. M. Grason, *Phys. Rev. E* **94**, 013003 (2016).
- 8 H. King, R. D. Schroll, B. Davidovitch, and N. Menon, *Proc. Natl. Acad. Sci. USA* **109**, 9716 (2012).
- 9 A. D. Cambou and N. Menon, *Proc. Natl. Acad. Sci. USA* **108**, 14741 (2011).
- 10 L. H. Dudte, E. Vouga, T. Tachi and L. Mahadevan, *Nat. Mater.* **15**, 583 (2016).
- 11 J. L. Silverberg, J-H. Na, A. A. Evans, B. Liu, T. C. Hull, C. D. Santangelo, R. J. Lang, R. C. Hayward and I. Cohen, *Nat. Mater.* **14**, 389 (2015).
- 12 M. Muthukumar, C. K. Ober, E. L. Thomas, *Science*, **277**, 1225 (1997).
- 13 P. Chaikin and T. Lubensky, *Principles of Condensed Matter Physics* (Cambridge Press, Cambridge, 1995).
- 14 S. Ganguly, P. Nath, J. Horbach, P. Sollich, S. Karmakar and S. Sengupta, *J. Chem. Phys.* **146**, 124501 (2017).
- 15 D. E. Discher, D. H. Boal, and S. K. Boey, *Phys. Rev. E* **55**, 4762 (1997).
- 16 D. H. Boal, U. Seifert, and A. Zilker, *Phys. Rev. Lett.* **69**, 3405 (1992).
- 17 H. Li and G. Lykotrafitis, *Biophys. J.* **102**, 75 (2012).
- 18 M. F. Thorpe and E. J. Garboczi, *Phys. Rev. B*, **42**, 8405 (1990).
- 19 D. H. Boal, U. Seifert, and J. C. Shillcock, *Phys. Rev. E*, **48**, 4274 (1993).
- 20 K. Binder and D. Heermann, *Monte Carlo Simulation in Statistical Physics: An Introduction, 5th Ed.* (Springer, Berlin, 2010).
- 21 M. P. Allen and D. J. Tildesley, *Computer Simulation of Liquids* (Oxford University Press, Oxford, 1987).
- 22 D. Frenkel and B. Smit, *Understanding Molecular Simulations* (Academic Press, San Diego, 2002).
- 23 P. Virnau and M. Müller, *J. Chem. Phys.* **120**, 10925 (2004).
- 24 S. Ganguly, S. Sengupta, P. Sollich, and M. Rao, *Phys. Rev. E* **87**, 042801 (2013).
- 25 S. Ganguly, S. Sengupta, and P. Sollich, *Soft Matter* **11**, 4517 (2015).
- 26 M. L. Falk and J. S. Langer, *Phys. Rev. E* **57**, 7192 (1998).
- 27 H. B. Callen *Thermodynamics and an Introduction to Thermostatistics, 2nd Ed.* (Wiley, New Jersey, 1985)
- 28 A. M. Ferrenberg and R. H. Swendsen, *Phys. Rev. Lett.* **61**, 2635 (1988).
- 29 R. Phillips *Crystals, defects and microstructures: Modeling across scales* (Cambridge Press, Cambridge, 2004).
- 30 R. Milkus and A. Zaccane, *Phys. Rev. B* **93**, 094204 (2016).
- 31 P. Nath, S. Ganguly, J. Horbach, P. Sollich, S. Karmakar and S. Sengupta, arXiv:1803.01671.
- 32 S. Plimpton, *J. Comp. Phys.* **117**, 1 (1995); (<http://lammps.sandia.gov>).
- 33 S. Ghosh *private communication*.